Zhang et al. *Zool. Res.* 2026, 47(3): 851−865
https://doi.org/10.24272/j.issn.2095-8137.2025.469
https://cstr.cn/32248.14.zr.2025.469

ZR | Zoological Research

Article Open Access

AI-aided design of multi-epitope peptide vaccine elicits cellular and humoral immunity to broad Omicron subvariants

Kai Zhang[1,2,#], Gangao Wang[3,#], Tingting Liu[2,#], Min Li[4,#], Longfei Ding[5], Yanqi Zhao[6], Jianqing Xu[5], Honglin Li[3], Jianhua Sun[2,7], Xinxin Zhang[6], Jing Chen[1,2], Guangyu Zhao[4,*], Xingchao Geng[8,*], Yiru Long[2,*], Likun Gong[1,2,7,*]

[1] *School of Chinese Materia Medica*, *Nanjing University of Chinese Medicine*, *Nanjing*, *Jiangsu* 210023, *China*

[2] *State Key Laboratory of Drug Research*, *Shanghai Institute of Materia Medica*, *Chinese Academy of Sciences*, *Shanghai* 201203, *China*

[3] *Innovation Center for AI and Drug Discovery*, *School of Pharmacy*, *East China Normal University*, *Shanghai* 200062, *China*

[4] *State Key Laboratory of Pathogen and Biosecurity*, *Academy of Military Medical Sciences*, *Beijing* 100071, *China*

[5] *Shanghai Public Health Clinical Center* & *Institutes of Biomedical Sciences*, *Fudan University*, *Shanghai* 201508, *China*

[6] *Shandong Laboratory of Yantai Drug Discovery*, *Bohai Rim Advanced Research Institute for Drug Discovery*, *Yantai*, *Shandong* 264117, *China*

[7] *Zhongshan Institute for Drug Discovery*, *Shanghai Institute of Materia Medica*, *Chinese Academy of Sciences*, *Zhongshan*, *Guangdong* 528400, *China*

[8] *Institute for Biological Product Control*, *National Institutes for Food and Drug Control*, *Beijing* 100176, *China*

ABSTRACT

Peptide vaccines offer a flexible, rapidly updatable platform for responding to SARS-CoV-2 antigenic drift. However, many candidates target a single epitope class, predominantly $CD4^+$/$CD8^+$ T-cell epitopes or short linear B-cell epitopes, limiting their capacity to induce both high-titer neutralizing antibodies and robust T-cell immunity. Here, to elicit potent humoral and cellular responses, we used AI-aided epitope prediction tools to analyze 18 Omicron subvariants and designed two candidate peptides from the RBD of XBB.1.5, designated LY54-XBB (L455–Y508) and P67-XBB (Y351–K378). *In silico* TCR-pMHC binding analysis and structural modeling showed that both peptides contained T-cell epitopes. The immunogenicity of the two peptide nanoemulsions was validated in murine and non-human primate (NHP) models. Mixed vaccination elicited RBD-binding, ACE2-blocking, and pseudovirus-neutralizing antibody responses, together with a Th1-biased cross-reactive cellular immune response, with no observable adverse reactions. Importantly, mixed vaccination protected the lungs of HLA-A2/DR1-hACE2 transgenic mice from the SARS-CoV-2 BA.5 variant challenge. In addition, *ex vivo* stimulation of hPBMCs from COVID-19 convalescent plasma donors confirmed that both peptides elicited antigen-specific $CD4^+$ and $CD8^+$ T-cell responses, validating the inclusion of effective T-cell epitopes. These complementary peptides, supported by both experimental and computational validation, represent promising rapidly updatable booster candidates. Our epitope-based pipeline provides a generalizable framework for vaccine design that may help sustain population immunity against SARS-CoV-2 and other antigenically diverse pathogens.

Keywords: Peptide vaccine; AI-aided design; SARS-CoV-2; T- and B-cell epitopes

INTRODUCTION

Peptide vaccines are chemically synthesized vaccines that differ from other vaccine platforms by identifying antigenic epitope peptides from pathogen proteins through *in vitro* screening or computational prediction strategies (Nelde et al., 2021; Shalash et al., 2021; Xiao et al., 2025). Because peptide vaccines target defined antigenic epitopes, they can help circumvent the adverse effects associated with non-protective epitopes and immune imprinting (Aguilar-Bretones et al., 2023). Furthermore, their fully chemical synthesis reduces the complexity and cost of production, quality control, and storage, facilitating rapid application in pandemic responses (Xiao et al., 2025). During the coronavirus disease 2019 (COVID-19) pandemic, peptide vaccines have

Received: 26 December 2025; Accepted: 08 January 2026; Online: 09 January 2026

Foundation items: This work was supported by the Strategic Priority Research Program, Chinese Academy of Sciences (XDB1310302), National Key Research and Development Program of China (2022YFC2304105), National Natural Science Foundation of China (82341039), Postdoctoral Fellowship Program of CPSF (GZB20230797), and Zhongshan Municipal Bureau of Science and Technology (CXTD2023010)

[#]Authors contributed equally to this work

*Corresponding authors, E-mail: zhaoguangyu@bmi.ac.cn; gengxch@nifdc.org.cn; s18-longyiru@simm.ac.cn; lkgong@simm.ac.cn

demonstrated protective potential in clinical studies (Ryzhikov et al., 2023; Tandler et al., 2024; Wang et al., 2022).

Despite the precision of antigenic epitopes, epitope selection, especially the balance between linear and conformational B-cell epitopes and the inclusion of $CD4^+$ and $CD8^+$ T-cell epitopes, is a major determinant of whether a peptide vaccine elicits high-quality humoral and cellular immunity (Malonis et al., 2020; Nelde et al., 2021). However, most early peptide candidates emphasized only a single epitope class. For example, EpiVacCorona, a short linear B-cell epitope peptide vaccine, became the first peptide vaccine to receive emergency use authorization in October 2020 (Ryzhikov et al., 2023), but its neutralizing antibody test results and efficacy have been questioned (Barchuk et al., 2022; Matveeva & Ershov, 2022). CoVac-1, a T-cell-focused peptide vaccine, elicited durable interferon (IFN)-γ-producing $CD4^+$ and $CD8^+$ T-cell responses in healthy volunteers (Tandler et al., 2024) but was not designed to induce high-titer spike-specific neutralizing antibodies (Heitmann et al., 2022), which may have contributed to its limited clinical efficacy.

For peptide vaccine design, these observations, together with methodological reviews, suggest that strategies integrating neutralizing B-cell determinants with $CD4^+$/$CD8^+$ T-cell epitopes, or preserving conformational B-cell epitopes, together with appropriate adjuvants and delivery systems, are more likely to yield coordinated humoral and cellular protection against rapidly mutating pathogens (Long et al., 2022; Malonis et al., 2020; Smith et al., 2021). However, this design approach still requires systematic development and extensive validation.

Here, to advance a generalizable, variant-resilient multi-epitope design strategy, we employed a comprehensive artificial intelligence (AI)-aided epitope prediction approach, which is recognized for accelerating vaccine development and reducing failure rates (Villanueva-Flores et al., 2025), with dual experimental and computational validation focused on the receptor binding domain (RBD) of XBB.1.5. Specifically, we screened T-cell and B-cell epitopes across 18 Omicron subvariants using sequence and structural criteria and prioritized two complementary peptides, LY54-XBB (L455–Y508) and P67-XBB (Y351–K378), on the basis of predicted immunodominance and structural accessibility. We then applied a dual-validation framework: (i) *in silico* human-translational assessment by integrating a COVID-19 patient-derived T-cell receptor (TCR) repertoire database with TCR-peptide-major histocompatibility complex (TCR-pMHC) binding prediction and structural modeling to prioritize epitopes with high translational potential; (ii) *in vivo* immunogenicity and safety assessment in murine and NHP models to determine breadth and quality of humoral and cellular responses; (iii) *in vivo* protective efficacy evaluation in MHC-humanized murine models; and (iv) *ex vivo* validation of T-cell epitope content using peripheral blood mononuclear cells (PBMCs) from COVID-19 convalescent plasma (CCP) donors to detect antigen-specific cellular immune responses. This study demonstrates a rapidly updatable method for identifying complementary peptide candidates that together elicit neutralizing antibody and T-cell responses, offering a promising modular approach for rapidly updatable boosters against immune-evasive severe acute respiratory syndrome coronavirus 2 (SARS-CoV-2) variants and other antigenically diverse pathogens.

MATERIALS AND METHODS

Animals and ethical statement

C57BL/6 mice were purchased from Shanghai Bikai Keyi Biotechnology Co., Ltd. (Experimental Animal Production License No. SCXK (Hu) 2023-0009) and maintained in the specific pathogen-free (SPF) animal laboratory of Shanghai Institute of Materia Medica (SIMM), Chinese Academy of Sciences. Mice experiments were approved by the Institutional Animal Care and Use Committee (IACUC) of SIMM (Approval No. 2024-06-GLK-65). Cynomolgus monkeys were maintained under Association for Assessment and Accreditation of Laboratory Animal Care (AAALAC) accredited Good Laboratory Practice (GLP) conditions, and the corresponding procedures were approved by the IACUC of SIMM (Approval No. 2024-08-CDSER-36). HLA-A2/DR1-hACE2 transgenic mice were housed in a biosafety level-3 facility. All infectious experiments were performed in accordance with the standard operating procedures of the approved biosafety level-3 facility and were approved by the Animal Experiment Committee of Laboratory Animal Center, Academy of Military Medical Sciences (Approval No. IACUC-IME-2022-044).

Cells and ethical statement

PBMCs from cynomolgus monkeys were isolated under sterile conditions and cultured in RPMI-1640 medium (Meilunbio, China) containing 1% penicillin/streptomycin (Gibco, USA) and 10% heat-inactivated fetal bovine serum (FBS; Life Technologies, USA). Human angiotensin-converting enzyme 2 (hACE2)-293T cells were cultured in DMEM medium (Meilunbio, China) containing 1% penicillin/streptomycin and 10% heat-inactivated FBS. Cells were maintained at 37°C in a humidified incubator with 5% CO_2. Human PBMCs (hPBMCs) from CCP donors were provided by Milecell Biological Science & Technology Co., Ltd., with institutional ethical approval (Approval No. Z-ZJMS-21-10-001), and cultured in complete RPMI-1640 medium.

Epitope peptide prediction

The RBD sequences (residues 319–541) of the SARS-CoV-2 spike glycoprotein were obtained from GISAID (https://gisaid.org/). Human MHC class II binding affinities were predicted using NetMHCIIpan 4.3, MHC class I peptide binding was assessed using NetMHCpan 4, and linear B-cell epitopes within the RBD were mapped using BepiPred 3.0 (Clifford et al., 2022; Nilsson et al., 2023; Reynisson et al., 2020). Structural representations of the RBD-ACE2 complex (PDB ID: 8JYP) were generated in PyMOL to illustrate key interaction residues. The secondary structures of epitopes were predicted using AlphaFold 3 (Abramson et al., 2024).

TCR-pMHC binding prediction

First, NetMHCpan 4.1 was used to predict the binding affinity between peptides (8-mer to 11-mer) and MHC class I molecules. Subsequently, the binding strength of pMHC to TCR (Schultheiß et al., 2020) was predicted using PISTE (Feng et al., 2024). The top three ranked pMHC-TCR triples for both the P67-XBB and LY54-XBB groups were selected based on prediction scores. The 3D structures of these triples were predicted using TCRmodel (Yin et al., 2023). Interactions between the pMHC and the TCR were visually examined using PyMOL. Finally, interface characterization was performed using CoCoMaps 2.0 (Vangone et al., 2011) to extract residue contacts, hydrogen bonds, salt bridges, hydrophobic contacts, and interface surface metrics.

Additional information on the modeling software and algorithms is provided in Supplementary Table S1.

Peptide synthesis

Peptides were synthesized by Hybio Pharmaceutical Co., Ltd. using solid-phase peptide synthesis (SPPS). Crude products were purified by preparative reversed-phase C18 high-performance liquid chromatography (RP-HPLC) to yield white powders. The purity of the final product (>90%) was confirmed by analytical RP-HPLC, and molecular identity was validated by high-resolution mass spectrometry (HRMS).

Vaccination for mice and cynomolgus monkeys

Female C57BL/6 mice (6–8 weeks old) were randomized into three groups (*n*=5). Peptides (LY54-XBB or P67-XBB, 50.0 μg/mouse) were emulsified 1:1 (v/v) with incomplete Freund's adjuvant (IFA; Sigma-Aldrich, USA) and immunized intramuscularly on days 0, 7, and 14. Blood samples were collected according to the experimental schedule.

For preliminary immunogenicity assessment, four monkeys were randomized into two groups (saline; LY54-XBB [1.0 mg]+P67-XBB [0.5 mg], *n*=2). In the formulation evaluation, sixteen monkeys were randomized into four groups (saline; LY54-XBB-L [0.4 mg]; LY54-XBB-H [0.8 mg]; or LY54-XBB-L+P67-XBB [0.4+0.2 mg], *n*=4). The two peptides were administered at equal molar concentrations. Monkeys were immunized with a vaccine formulated in saline or with peptides plus the developed F2 adjuvant (Long et al., 2022) on days 0, 14, and 28. Blood samples were collected according to the experimental schedule.

Female HLA-A2/DR1-hACE2 mice (6–8 weeks old) were randomized into three groups (PBS, LY54-XBB [50.0 μg], and LY54-XBB+P67-XBB [50.0+25.0 μg]; *n*=5), and immunized on days 0, 14, and 28. F2 adjuvant was used in the formulations. Mice were challenged with live BA.5 virus 14 days after the third immunization.

Detection of serum SARS-CoV-2 RBD-specific antibody

96-well plates (ThermoFisher, USA) were coated overnight at 4°C with recombinant SARS-CoV-2 RBD (1 μg/mL, XBB, BA.4/BA.5/BA.5.2, BA.4.6/BF.7, BA.2.86, or JN.1; SinoBiological, China) or peptide (3 μg/mL) in PBS (pH 7.4; Yuchun, China). Plates were washed three times with PBST (PBS+0.1% Tween-20) and blocked for 1 h at 37°C with PBST containing 3% BSA (Yeasen, China). Serum samples were serially diluted (starting at 1:100) in PBST+1% BSA, added to each well, and incubated for 1 h at 37°C. After three washes, either goat anti-mouse IgG-horseradish peroxidase (HRP) (1:10 000; Abcam, UK) or Protein A-HRP (1:10 000; GenScript, China) was applied for 1 h at 37°C. Plates were washed again, and tetramethylbenzidine (TMB; SeraCare, USA) substrate was added and incubated in the dark for 20 min. The reaction was terminated with 2 mol/L H_2SO_4, and optical density (OD) was measured at 450 nm using a microplate reader.

Detection of serum SARS-CoV-2 ACE2-RBD blocking antibody

96-well plates were coated overnight at 4°C with human ACE2 (4 μg/mL; GenScript, China) in PBS (pH 7.4). Plates were washed three times with PBST and blocked for 1 h at room temperature with PBST containing 3% BSA. Serum samples were serially diluted (starting at 1:10) in PBST+1% BSA and pre-incubated for 1 h at 37°C with an equal volume of either RBD-HRP conjugate (1:5 000; GenScript, China) or His-tagged RBD (0.25 μg/mL). The serum-RBD mixtures were then transferred to ACE2-coated wells and incubated for 1 h at 37°C. After washing, the TMB substrate was added and incubated in the dark for 20 min. The reaction was stopped with 2 mol/L H_2SO_4, and OD_{450} values were recorded. Inhibition rates were calculated relative to the blank serum control.

Pseudovirus neutralization assay

The pseudoviruses were obtained from a previous study (He et al., 2021), and experiments were performed at the Shanghai Public Health Clinical Center (SPHCC). In brief, heat-inactivated sera were serially diluted in complete DMEM and mixed 1:1 (v/v) with 50 μL of pseudovirus. After incubation for 1 h, hACE2-293T cells (4×10^4 cells/mL) were added to each mixture. Plates were incubated for 48 h, then luciferase activity was measured using the Bright-Glo Luciferase Assay System (Promega) on a GloMax 96 luminometer. The 50% pseudovirus neutralization titers ($pVNT_{50}$) were defined as the highest serum dilution yielding a 50% reduction in relative light units compared with virus-only control wells, following background subtraction.

Detection of Th1/Th2 cytokine from culture supernatants

PBMCs from cynomolgus monkeys were isolated using Ficoll-Paque PREMIUM (Cytiva, China) and resuspended in culture medium at 2×10^6 cells/mL. PBMCs were stimulated with peptides (20 μg/mL) for 24 h or 48 h. Supernatants were harvested for cytokine quantification. helper T-cell (Th) 1/Th2 cytokines (interleukin [IL]-2, tumor necrosis factor [TNF]-α, IFN-γ, IL-4, IL-5, and IL-10) were measured using a Cytometric Bead Array (CBA) kit (BD, USA) according to the manufacturer's instructions. Samples were subsequently analyzed using a flow cytometer (Agilent, USA), and data were processed using NovoExpress.

Enzyme-linked immunospot (ELISpot) assay

IFN-γ ELISpot assays were performed using ELISpot Flex kits (Mabtech, Sweden) according to the manufacturer's protocol. Briefly, PVDF membranes (Millipore, China) were coated with capture antibody overnight at 4°C and blocked before use. Cells were plated at 5×10^5 cells per well and stimulated with recombinant human IL-2 protein (rhIL-2, 10 or 100 U/mL; Genscript, China) and peptides (LY54-XBB [40 μg/mL] or mixed LY54-XBB&P67-XBB [40 μg/mL total]), or with rhIL-2 (100 U/mL) and RBD (20 μg/mL, from BA.2.86, JN.1, or XBB). Negative controls received no antigen stimulation; positive controls were stimulated with phytohemagglutinin (PHA, 5 μg/mL; Yeasen, China). After incubation for 24 or 48 h at 37°C with 5% CO_2, plates were developed according to the kit instructions, and spots were counted using a CTL ImmunoSpot Analyzer (Cellular Technologies, USA).

IgG ELISpot assays were performed using ELISpot Flex kits (Mabtech, Sweden) according to the manufacturer's protocol. After PBMCs were co-cultured with peptides for 5 d, cells were collected, resuspended, and transferred onto PVDF membranes coated with IgG capture antibodies. IgG spots were detected after 24 h using the kits.

Mouse challenge experiments

For intranasal infection, HLA-A2/DR1-hACE2 transgenic mice were anesthetized with sodium pentobarbital (50 mg/kg) via the intraperitoneal route and then intranasally infected with 3×10^3 50% tissue culture infectious doses ($TCID_{50}$) of the SARS-CoV-2 BA.5 variant. Mice were monitored daily and sacrificed on day 5 post-infection for tissue processing.

Measurement of viral RNA loads

Viral RNA was extracted from each sample using an RNeasy mini kit (Qiagen, Germany) according to the manufacturer's protocol. Viral RNA was quantified by reverse transcription quantitative PCR (RT-qPCR) targeting the E gene of the SARS-CoV-2 BA.5 variant. RT-qPCR was performed using a One Step Prime Script RT-PCR kit (Takara, Japan) with the following primers and probe: E_Sarbeco forward primer, ACAGGTACGTTAATAGTTAATAGCGT; E_Sarbeco FAM-BBQ probe, FAM-ACACTAGCCATCCTTACTGCGCTTCG-BBQ; and E_Sarbeco reverse primer, ATATTGCAGCAG TACGCACACA.

Histopathological studies

The lungs of sacrificed mice were fixed in 10% neutral buffered formalin, followed by dehydration and paraffin embedding. Each embedded block was then longitudinally sectioned at a thickness of 4 μm. Tissue sections were processed and stained with hematoxylin and eosin (H&E) using standard protocols for subsequent light microscopic evaluation. Lung damage was semi-quantitatively assessed under microscopy based on established criteria (Sun et al., 2020; Xue et al., 2022). Lungs were evaluated for lesions, including airway epithelium loss, exudates, bronchial epithelial hyperplasia, vascular inflammatory cell margination/endothelial hyperplasia, peribronchial inflammation and edema, septal thickening/inflammation, alveolar inflammation, alveolar edema/hemorrhage, extent of alveolar damage, pulmonary consolidation, and alveolar epithelial hyperplasia. Each type of pulmonary lesion was assigned a severity grade on a 1–5 scale as follows: 0=no lesions; 1=minimal, focal to multifocal, inconspicuous; 2=mild, multifocal, prominent; 3=moderate, multifocal, prominent; 4=marked, multifocal or coalescing, lobar; 5=severe, extensive, or diffuse, multilobar, with consolidation. Intermediate severity grades were also assigned as needed and these grades were then converted to weighted semi-quantitative scores as follows: 0=0; 1=1; 1.5=8; 2=15; 2.5=25; 3=40; 3.5=60; 4=80; 4.5=90; 5=100. These lesion scores were used to calculate mean severity scores for each experimental group.

Detection of intracellular Th1/Th2 cytokines

Human PBMCs were co-incubated with peptides (40 μg/mL) and brefeldin A solution (BFA, diluted to 1X; Biolegend, USA) for 6 h. Cells were collected and blocked with human Fc Block (BD, USA), then incubated at 4°C for 25 min with surface marker antibodies, including PE Mouse Anti-Hu CD3 (BD, USA), PerCP-Cy5.5 Mouse Anti-Hu CD4 (BD, USA), and FITC Mouse Anti-Hu CD8 (BD, USA). After permeabilization at 4°C for 30 min using Cytofix/Cytoperm Fixation/Permeabilization kit (BD, USA), samples were incubated at 4°C for 25 min with intracellular antibodies, including APC Rat Anti-Hu IL-2 (BD, USA), Brilliant Violet 605 anti-Hu IFN-γ (Biolegend, USA), BV421 Mouse Anti-Hu TNF-α (BD, USA), Rat Anti-Hu IL-4 (BD, USA), and PE/Cyanine7 anti-Hu IL-6 Antibody (Biolegend, USA). Antibody volumes were used as recommended in the manufacturer's instructions. Detection was performed as described above.

Analysis of hematologic and biochemical parameters

Venous blood was collected from cynomolgus monkeys into EDTA tubes and processed immediately. Hematological parameters were analyzed using an ADVIA 2120i hematology analyzer (Siemens, Germany). Plasma was separated by centrifugation and analyzed for biochemical parameters using a Cobas C501 biochemical analyzer (Roche, Switzerland).

Statistical analysis

All statistical analyses were performed using GraphPad Prism v.9.5.1, Origin 2025, or R v.4.5.1 with the ggplot2 package. Data are presented as mean±standard error of the mean (SEM). For comparisons between two groups, unpaired two-tailed *t*-tests were used. For multiple group comparisons, one-way ANOVA followed by Tukey's or Dunnett's post-hoc test was applied as appropriate. Statistical significance was defined as follows: *: $P<0.05$; **: $P<0.01$; ***: $P<0.001$; ****: $P<0.0001$; ns: not significant. In the figures, asterisks (*) denote statistical significance compared with the control group, while hash symbols ($^{\#}$) indicate significance between different experimental groups.

RESULTS

AI-aided design of antigenic peptides

As SARS-CoV-2 continues to evolve, previous vaccines have struggled to cope with Omicron subvariants, prompting us to develop an immunogen based on updated epitopes. We obtained the RBD protein sequence of XBB.1.5, which has been reported to possess strong immune escape capability (Yue et al., 2023), for T-cell and B-cell epitope prediction. Here, we employed an AI-aided antigenic peptide screening and evaluation strategy that integrates sequence information, structural information, and predictions of cellular and humoral immune epitopes.

We screened for epitopes exhibiting high binding affinity (score>0.426) for both $CD4^{+}$ and $CD8^{+}$ T cells using NetMHCpan and NetMHCIIpan (Supplementary Figure S1; Figure 1A). Using BepiPred, we found that these segments overlapped with B-cell epitopes (Figure 1B). The results indicated that segments W353–F392, G447–D467, Q493–V510, and P527–K537 within the RBD of XBB.1.5 represented potential comprehensive immunodominant epitopes. Long peptides have been reported to exhibit stronger immunogenicity than short peptides (Chen et al., 2020). Considering previously reported neutralizing epitopes and SARS-CoV-2 receptor-binding motif (RBM) domains (Piccoli et al., 2020; Shi et al., 2020), we linearly combined the peptide segments and named the resulting peptides P67-XBB (Y351–K378) and LY54-XBB (L455–Y508) (Figure 1C).

In addition, we obtained the RBDs of 18 Omicron subvariants for epitope prediction using AI-aided tools. Although point mutations exist among variants (Supplementary Figure S2A), L455–Y508 and Y351–K378 consistently served as high-affinity epitopes for $CD4^{+}$ (Supplementary Figure S2B) and $CD8^{+}$ T cells (Supplementary Figure S2C), as well as B cells (Supplementary Figure S3D).

Structurally, the L455–Y508 domain overlaps with the class 1 and class 2 neutralizing epitopes (Wibmer et al., 2021) and directly interfaces with hACE2 in XBB.1.5 (Figure 1D). Structural predictions of peptides further confirmed high conformational conservation of the L455–Y508 among Omicron subvariants (RMSD≤0.708 Å; Figure 1E). Given that long linear epitopes can adopt conformations capable of inducing neutralizing antibodies (Li et al., 2014), we hypothesized that antibodies induced by LY54-XBB could confer broad protection against Omicron subvariants through steric hindrance.

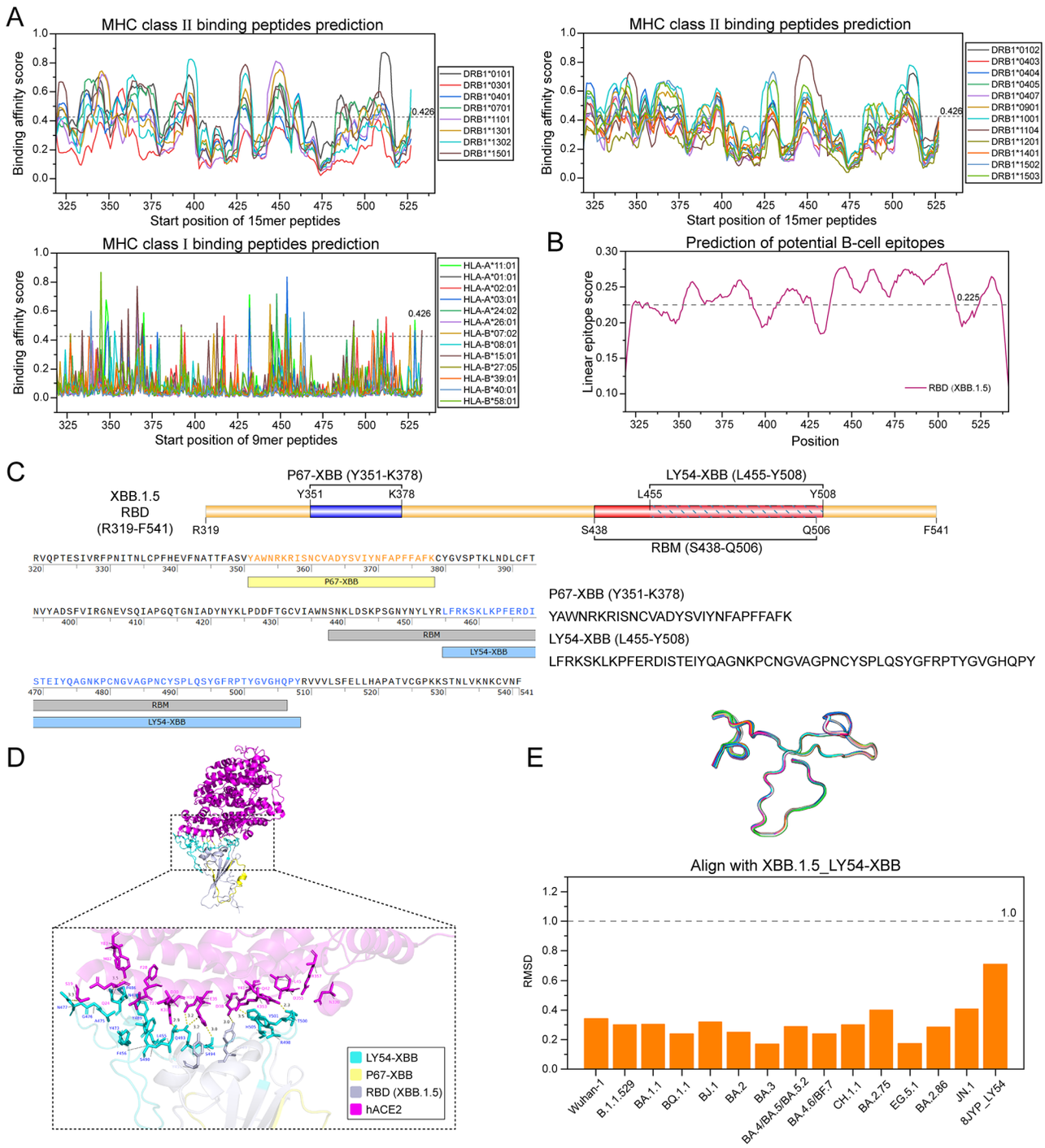

Figure 1 Design of epitope peptides

A: Potential binding peptides of MHC class I and II molecules across frequent HLA alleles were predicted by NetMHCpan and NetMHCIIpan. B: Potential B-cell epitope peptides were predicted by BepiPred. C: Amino acid sequences of LY54-XBB and P67-XBB in the XBB.1.5 RBD. D: Locations of LY54-XBB and P67-XBB at the interaction interface between $RBD_{XBB.1.5}$ and hACE2 visualized by PyMOL. Data were obtained from the Protein Data Bank (PDB; code 8JYP). E: The LY54 conformations derived from multiple Omicron subvariants were predicted by AlphaFold 3, with alignment and visualization performed using PyMOL.

In summary, AI-based immunogenic epitope prediction demonstrated that LY54-XBB and P67-XBB are potential immunodominant candidate peptides containing T-cell and B-cell epitopes.

TCR-pMHC binding analysis evaluates the cellular immune activation potential of candidate peptides

TCRs recognize complexes of foreign peptides and MHC molecules to initiate T-cell signaling and adaptive immunity (Yin et al., 2023). To further assess the ability of P67-XBB and LY54-XBB to elicit cellular immunity, we predicted interactions among TCR-pMHC triples. A curated database of 353 999 TCR sequences derived from COVID-19 patient repertoires (during infection or after recovery) was used as the TCR background for prediction (Schultheiß et al., 2020). Using PISTE, a previously developed model for predicting TCR-pMHC triples (Feng et al., 2024), we analyzed peptide segments (8-mer to 11-mer) derived from P67-XBB and LY54-XBB. Several peptides derived from P67-XBB and LY54-XBB,

such as P67-DYSVIYNF (8D364), P67-DYSVIYNFAPF (11D364), and LY54-CYSPLQSYGF (10C488), exhibited binding to most TCRs with an average binding score exceeding 0.9 (Figure 2A).

To compare overall TCR engagement, the top ten peptide fragments from each peptide, ranked by the number of

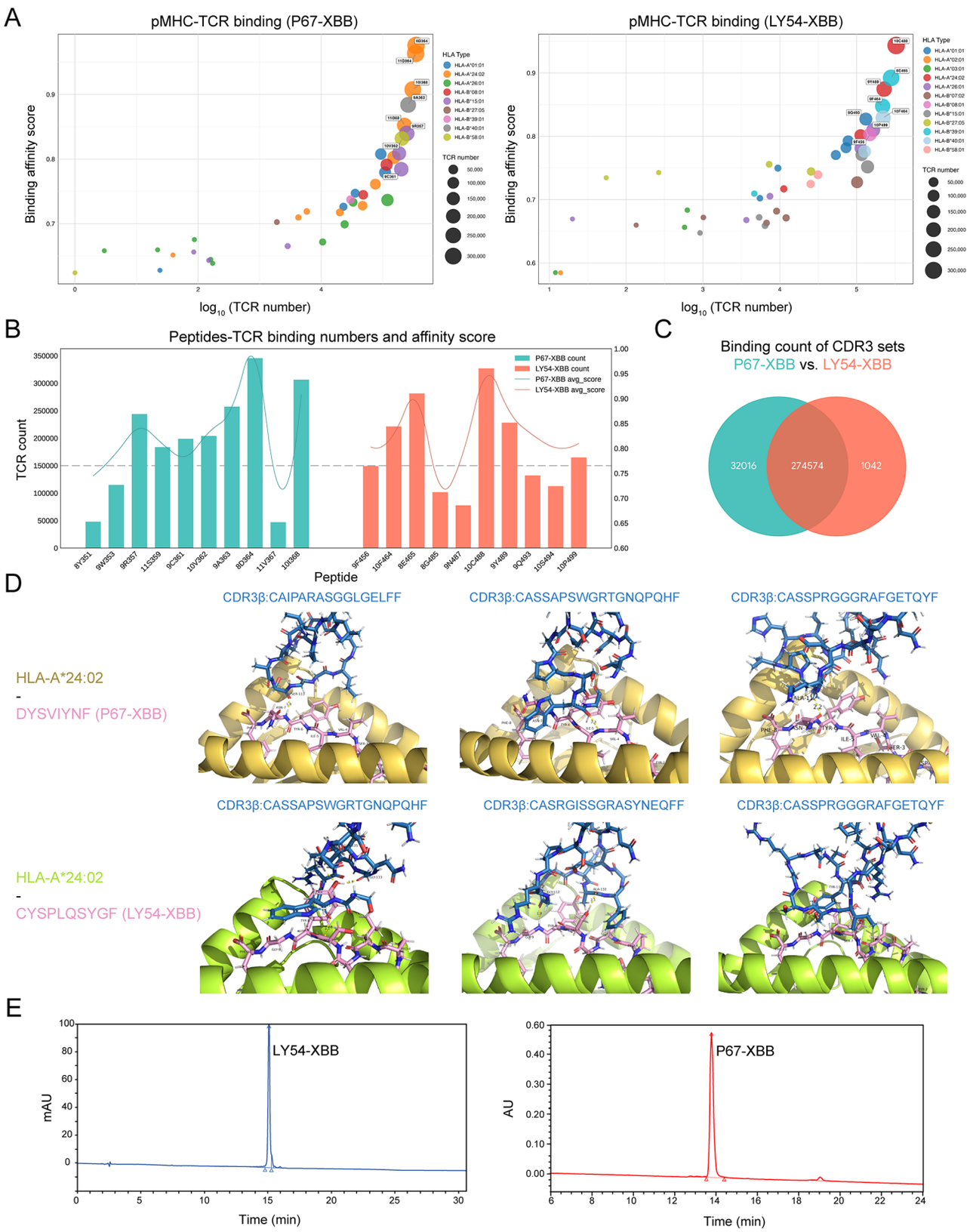

Figure 2 Prediction of peptide-induced cellular immunity and production of peptides

A: Peptide TCR-pMHC binding affinity scores were predicted using the PISTE model with a threshold of 0.5. B: Top 10 TCR binding scores for pMHCs of P67-XBB and LY54-XBB. C: Complementary HLA restriction and an expanded unique clonotype repertoire are shown by a Venn diagram. D: Spatial interactions between peptide (pink)-MHC (yellow or green) complexes and TCRs (blue) were modeled using TCRmodel2. E: Purity of LY54-XBB and P67-XBB peptides analyzed by HPLC.

predicted TCR binders, were further analyzed. Seven P67-XBB and five LY54-XBB fragments were predicted to engage >150 000 TCRs (Figure 2B), indicating that both peptides contain $CD8^+$ T-cell epitopes. Repertoire and HLA-level analyses support a compensatory, non-additive relationship: P67-XBB was preferentially associated with HLA-B*58:01 and HLA-A*24:02, while LY54-XBB was enriched for HLA-B*39:01 and HLA-B*07:02 (Supplementary Figure S3). The two peptides shared a large clonotype core (*n*=274 574), but P67-XBB contributed substantially more unique clonotypes (*n*=32 016 vs. 1 042 for LY54-XBB) (Figure 2C), indicating that P67-XBB broadens recognition space across HLA backgrounds.

Based on the PISTE predictions, we selected pMHC HLA-A*24:02-DYSVIYNF (P67-8D364) and HLA-A*24:02-CYSPLQSYGF (LY54-10C488) for structural modeling. Using TCRmodel2 (Yin et al., 2023), based on the predicted binding scores, we generated structural models of the top three TCRs bound to the pMHC and inspected the intermolecular interfaces (Figure 2D). Interface characterization was performed with CoCoMaps 2.0 (Vangone et al., 2011). The results showed 9–21 peptide-TCRβ contacts and 5–11 peptide-TCRα contacts, suggesting CDR3β-dominated peptide contacts. In addition, each complex contained 1–7 peptide-TCRβ hydrogen bonds, 0–2 peptide-TCRα hydrogen bonds, and 1–3 significant hydrophobic contacts. No persistent salt bridges were detected under our geometric criteria (Supplementary Table S2). These results support the ability of the selected peptides to form stable TCR-pMHC interfaces at both conformational and molecular-interaction levels.

Further, the LY54-XBB and P67-XBB were subsequently synthesized by solid-phase peptide synthesis, followed by purification and validation by HPLC (Figure 2E) and HRMS (Supplementary Figures S4–S5), confirming their suitability for subsequent immunogenicity evaluation and vaccine development.

Immunogenicity assessment of LY54-XBB and P67-XBB in mice

To evaluate the immunogenicity of the candidate peptides, C57BL/6 mice were immunized with three doses of LY54-XBB or P67-XBB (50.0 μg/dose) peptides, and blood samples were collected (Figure 3A). Peptide-specific IgG in serum was induced in the LY54-XBB and P67-XBB groups, with IgG titers ($Tlog_{10}$=4.6 and 4.0, respectively) maintaining high levels at 238 days post-first immunization (Figure 3B). At peak immunogenicity (day 70), the RBD-specific IgG titers were significantly induced in the LY54-XBB group against XBB, BA.4/BA.5/BA.5.2, BA.4.6/BF.7, JN.1, and BA.2.86, whereas they were undetectable in the P67-XBB group (Figure 3C). Considering the previous evidence for high-affinity binding of P67-XBB to MHC-I/II molecules (Figure 1A), we hypothesize that, despite possessing a B-cell epitope, P67-XBB functions mainly as a T-cell epitope because it is located in an inaccessible region of the surface protein (Pompano et al., 2014; Su et al., 2021). Moreover, peptide-specific antibody subclasses IgG2b and IgG1 were induced in the vaccine groups, and the IgG2b/IgG1 ratios in the LY54-XBB (1.3) and P67-XBB (2.4) groups (Figure 3D) indicated a Th1-biased response (Fornefett et al., 2018). No significant body weight changes were observed across groups (Figure 3E). Collectively, these data demonstrate that both LY54-XBB and P67-XBB peptides possess favorable immunogenicity in mice.

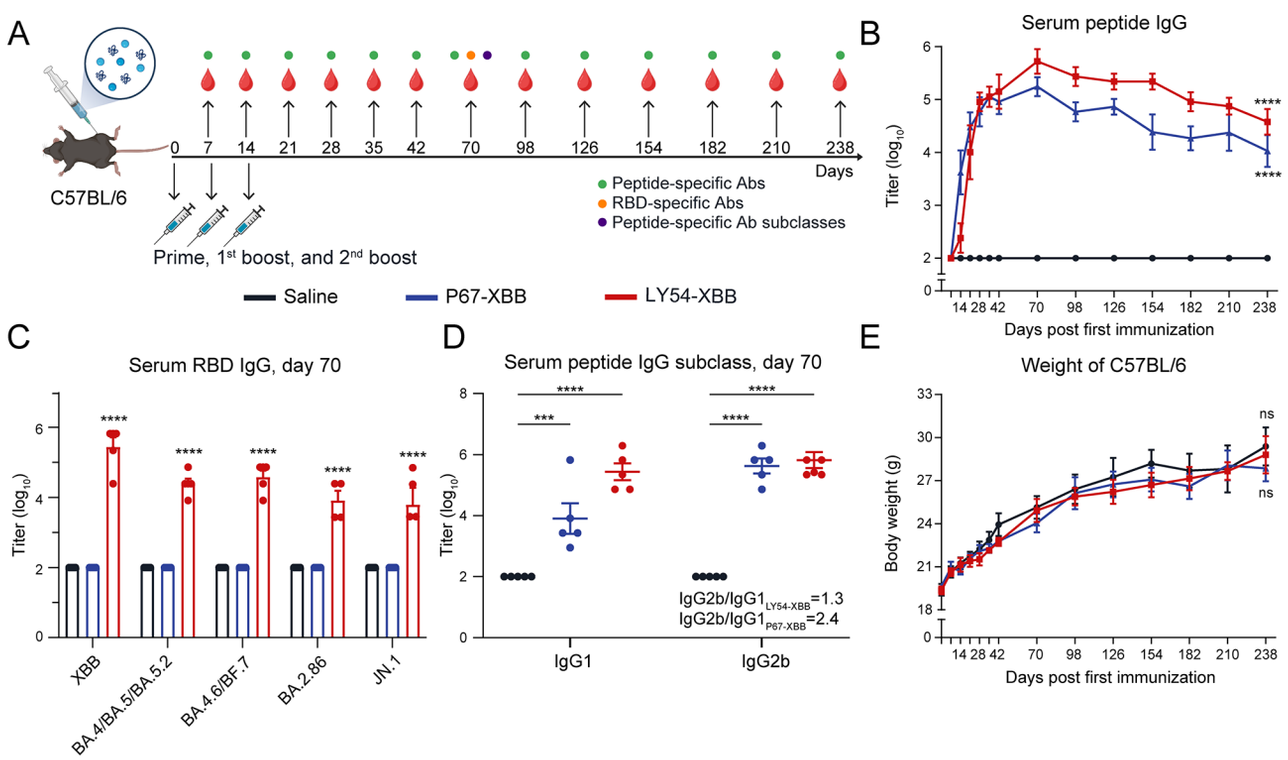

Figure 3 Immunogenicity assessment of LY54-XBB and P67-XBB peptides in C57BL/6 mice

A: Schedule of immunization for mice and blood collection (*n*=5). Antigen-specific antibodies were detected by indirect ELISA. B: Serum peptide-specific IgG antibodies were routinely detected (*n*=5). C-D: On day 70 post-first immunization, serum RBD-specific IgG and peptide-specific IgG1 and IgG2b were detected (*n*=5). The IgG2b/IgG1 ratio was calculated using the average of the IgG subclass titers in each group (*n*=5). E: Effect of peptide vaccines on body weight in mice (*n*=5). Data represent mean±SEM. For multiple group comparisons, one-way ANOVA followed by Tukey's or Dunnett's post-hoc test was applied as appropriate. ***: P<0.001; ****: P<0.0001; ns: Not significant.

Humoral immune responses of cynomolgus monkeys immunized with peptide vaccines

To preliminarily assess the immunogenicity of the mixed peptide vaccine, cynomolgus monkeys received three intramuscular immunizations with LY54-XBB (1.0 mg) and P67-XBB (0.5 mg) peptides, followed by blood sample collection (Figure 4A). The vaccine rapidly induced peptide-specific IgG antibodies, which peaked at day 28 post-first immunization ($Tlog_{10}$=7.3) and maintained stable titers through the study endpoint (Figure 4B). Consistent with the murine results, the LY54-XBB&P67-XBB formulation induced broad RBD-specific IgG against multiple Omicron subvariants, with log_{10} titers reaching 4.4, 4.4, 4.4, 4.2, and 4.2 for XBB, BA.4/BA.5/BA.5.2, BA.4/BF.7, BA.2.86, and JN.1, respectively (Figure 4C).

Notably, sera from the LY54-XBB&P67-XBB group exhibited robust ACE2-RBD blocking antibody activity at a serum dilution of 1:20, with inhibition rates reaching 81.5%, 75.0%, 59.0%, 51.5%, 45.5%, and 77.0% for Omicron, XBB, BA.4/BA.5/BA.5.2, BA.4/BF.7, BA.2.86, and JN.1, respectively, whereas saline controls showed no activity (Figure 4D). Some inter-animal variation was observed, potentially reflecting differences in initial immune activation or MHC polymorphism affecting peptide presentation and T-cell help, as documented in NHPs (Brochu et al., 2022; Heijmans et al., 2020). Furthermore, sera from the LY54-XBB&P67-XBB group demonstrated potent pseudovirus neutralization, with $pVNT_{50}$ values of 317, 38, and 98 against BA.5, XBB.1.5, and BF.7, respectively (Figure 4E). Together, these findings preliminarily indicate that the LY54-XBB&P67-XBB peptide vaccine induces broad humoral immunity against diverse Omicron subvariants.

Optimization of peptide vaccine formulations

To assess the effect of antigen dose and the contribution of the P67-XBB peptide to the immune response, the cynomolgus monkeys were immunized with either 0.4 mg (low dose, LY54-XBB-L) or 0.8 mg (high dose, LY54-XBB-H) of LY54-XBB, or with a combination of 0.4 mg LY54-XBB and

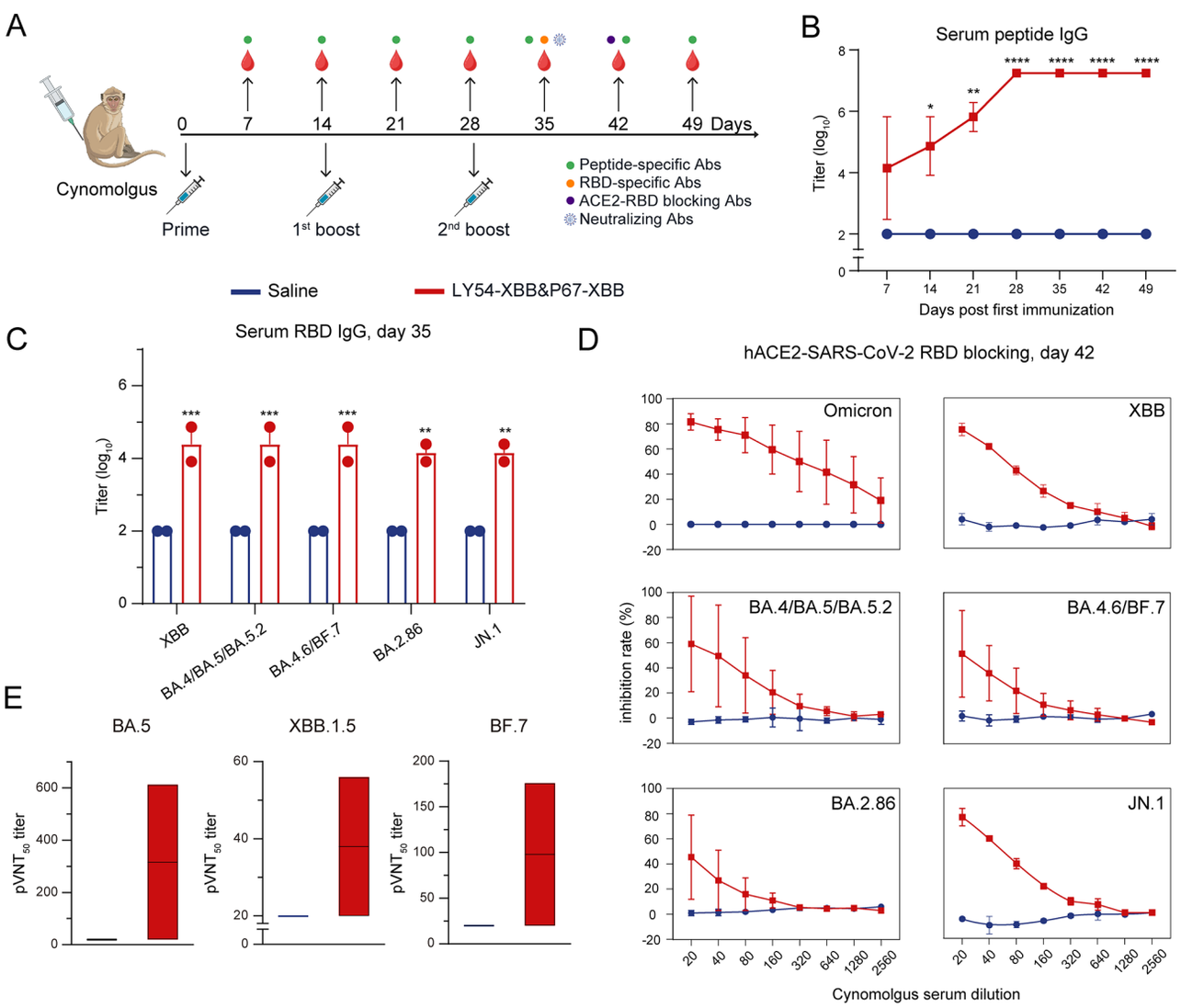

Figure 4 Humoral immune responses induced by LY54-XBB&P67-XBB formulation in cynomolgus monkeys

A: Schedule of immunization and blood collection in cynomolgus monkeys (*n*=2). Serum peptide-specific antibodies were detected by indirect ELISA. B: Serum peptide-specific IgG antibodies were routinely detected (*n*=2). C: On day 35 post-first immunization, serum RBD-specific IgG antibodies were detected (*n*=2). D: On day 42 post-first immunization, serum ACE2-RBD blocking antibodies were detected (*n*=2). E: On day 35 post-first immunization, serum neutralizing antibodies against pseudoviruses (BA.5, XBB.1.5, and BF.7) were detected (*n*=2). Data represent mean±SEM. For comparisons between two groups, unpaired two-tailed *t*-tests were used. **: P<0.01; ***: P<0.001; ****: P<0.0001.

0.2 mg P67-XBB (LY54-XBB-L&P67-XBB). Blood samples were collected as scheduled (Figure 5A). All vaccinated groups elicited strong and comparable peptide-specific IgG antibody responses (Figure 5B). However, both the LY54-XBB-H and LY54-XBB-L&P67-XBB groups induced higher ACE2-RBD blocking antibody levels than the LY54-XBB-L group (Figure 5C). At a 1:20 serum dilution, inhibition rates reached 48.3%, 63.3%, and 72.8% for the LY54-XBB-L, LY54-XBB-H, and LY54-XBB-L&P67-XBB groups, respectively. Pseudovirus neutralization assays further revealed that the LY54-XBB-L&P67-XBB group elicited the highest $pVNT_{50}$ titers against BA.5, XBB.1.5, and BF.7, reaching 133, 126, and 58, respectively (Figure 5D). These results indicate that both antigen dose and the inclusion of P67-XBB enhance the immunogenicity of the peptide vaccine. Although P67-XBB may not directly induce neutralizing antibodies, it appears to synergize with LY54-XBB to significantly potentiate neutralizing antibody responses.

Cellular immune responses of cynomolgus monkeys immunized with peptide vaccines

To evaluate the cellular immune responses, PBMCs were isolated on day 63 post-first immunization. Cytokine levels in supernatants collected after 24–48 h of peptide stimulation were quantified by flow cytometry. Both the LY54-XBB-H and LY54-XBB-L&P67-XBB groups exhibited markedly enhanced secretion of IL-2 and TNF-α compared to the saline control, with the LY54-XBB-L&P67-XBB combination eliciting the strongest response (Figure 6A, B). These data indicate that the peptide vaccines induced a Th1-biased cellular immune response.

IFN-γ-mediated cellular immunity is critical for protection against SARS-CoV-2 infection and has been associated with cross-variant immunity (Wang et al., 2023). Peptide-specific T-cell responses were assessed by ELISpot assay after 24 h stimulation with peptides. All peptide-vaccinated groups exhibited increased numbers of IFN-γ-secreting cells compared with the saline control (Figure 6C). Similarly, after

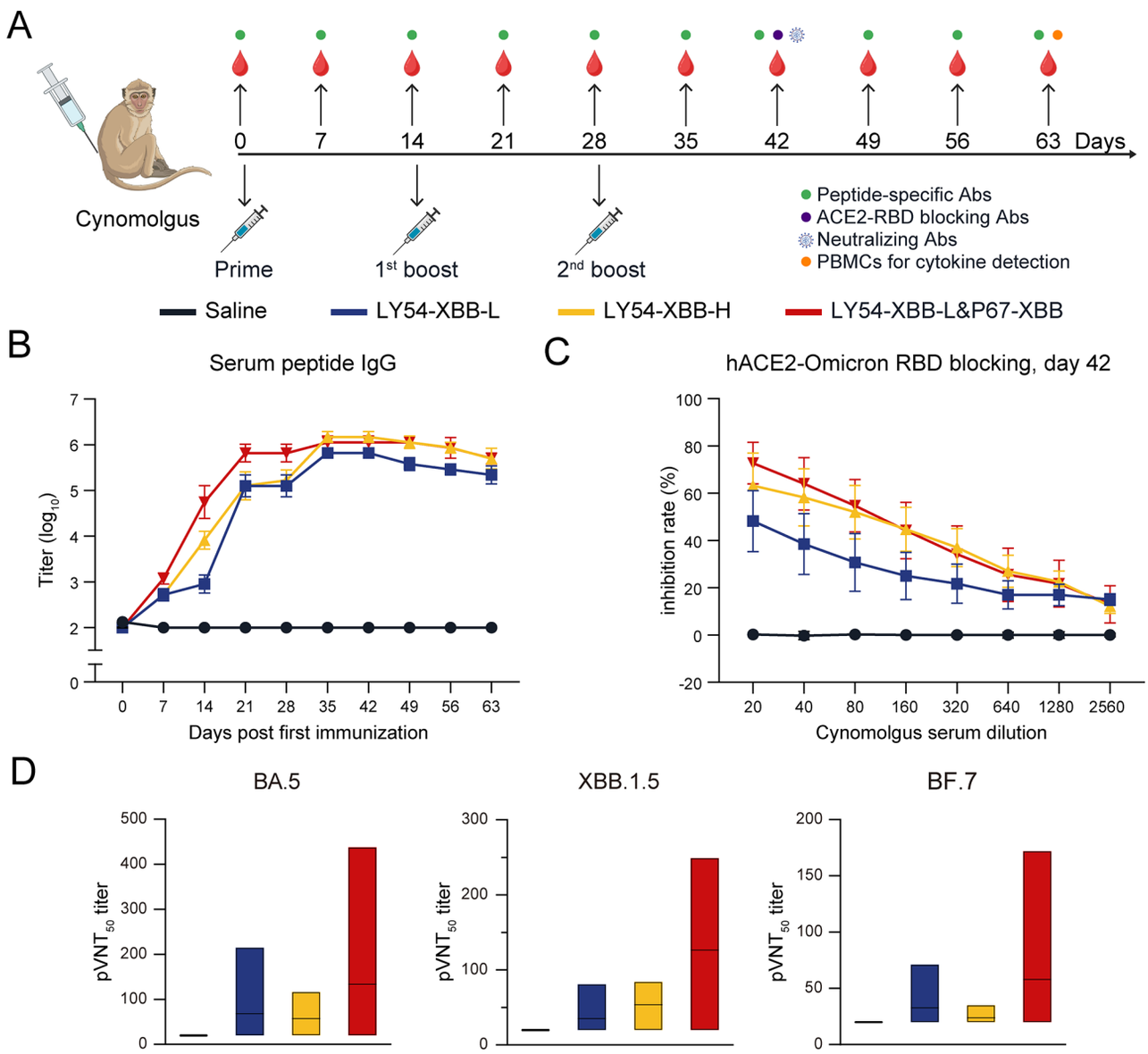

Figure 5 Humoral immune responses induced by differently formulated peptide vaccines in cynomolgus monkeys

A: Schedule of immunization and blood collection in cynomolgus monkeys (*n*=4). B: Serum peptide-specific IgG antibodies were routinely detected (*n*=4). C: On day 42 post-first immunization, serum ACE2-RBD blocking antibodies were determined (*n*=4). D: On day 35 post-first immunization, serum neutralizing antibodies against pseudoviruses (BA.5, XBB.1.5, and BF.7) were detected (n=4). Data represent mean±SEM.

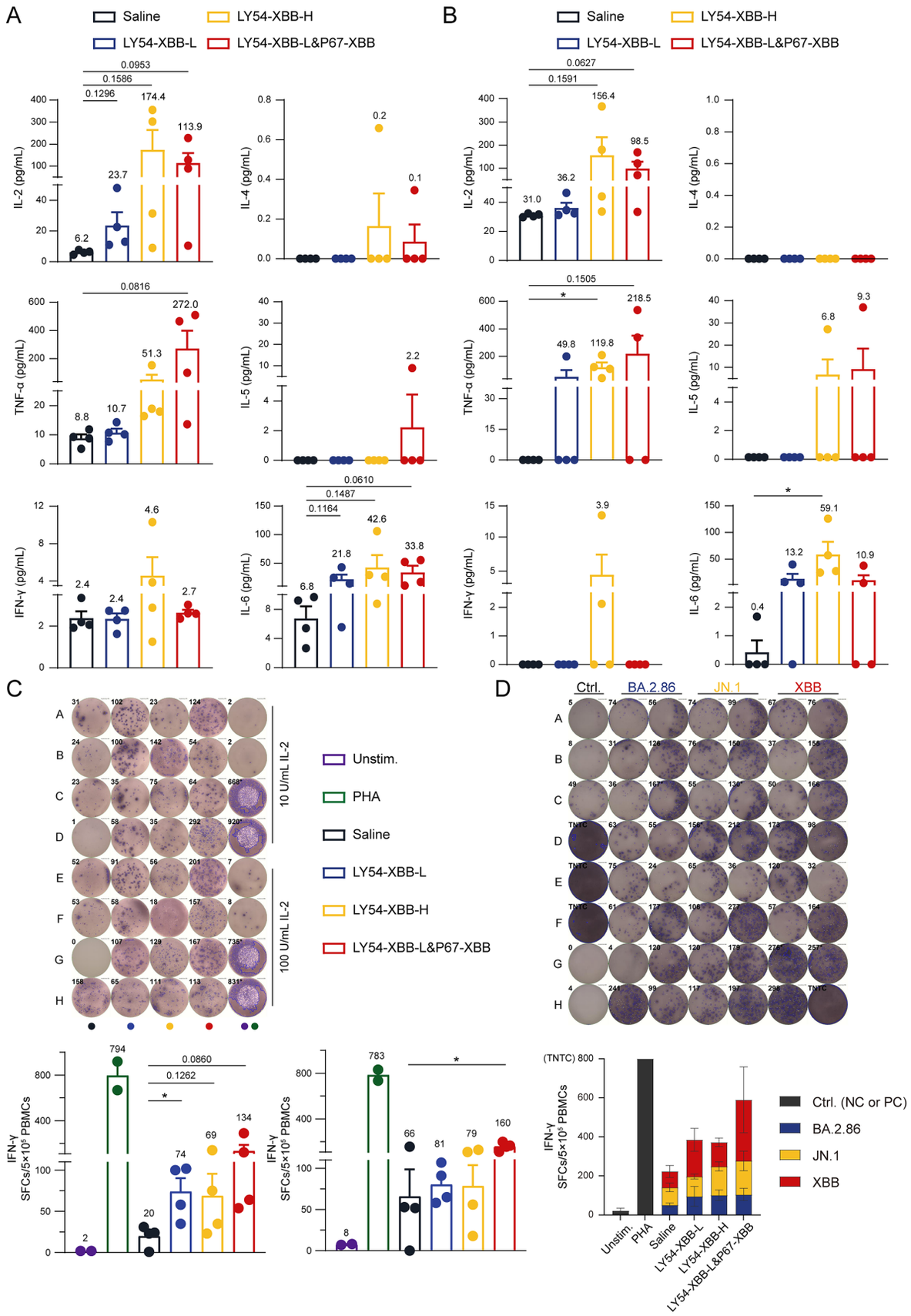

Figure 6 T-cell immune responses induced by peptide vaccines

A-B: On day 63 post-first immunization, PBMCs were isolated for the subsequent experiments (*n*=4). Th1/Th2 cytokines in PBMC supernatants after 24–48 h of peptide stimulation were detected using CBA kits and quantified by flow cytometry. C: IFN-γ secreted by PBMCs after 24 h of co-culture with peptides was detected by ELISpot (*n*=4). D: IFN-γ secreted by PBMCs after 48 h of co-culture with RBD derived from XBB, JN.1, or BA.2.86 was detected by ELISpot assay (*n*=4). Data represent mean±SEM. For multiple group comparisons, one-way ANOVA followed by Tukey's or Dunnett's post-hoc test was applied as appropriate. *: *P*<0.05.

48 h stimulation of PBMCs with BA.2.86, JN.1, or XBB RBD, all peptide-vaccinated groups showed increased numbers of IFN-γ-secreting cells compared with the unstimulated control, indicating enhanced cross-reactive cellular immune responses (Figure 6D). In addition, PBMCs from these groups exhibited more IgG-secreting cells (Supplementary Figure S6), with the highest number of spots detected in the LY54-XBB-L&P67-XBB group.

In summary, the candidate peptide vaccines designed against the XBB.1.5 RBD epitope elicited a Th1-biased cellular immune response. Importantly, the LY54-XBB-L&P67-XBB peptide vaccine demonstrated the highest immunogenicity, underscoring the contribution of P67-XBB.

Protective efficacy against BA.5 challenge in HLA-A2/DR1-hACE2 mice

To evaluate whether the peptide vaccine induced a protective immune response, HLA-A2/DR1-hACE2 mice were randomized into three groups with five mice in each group: PBS, LY54-XBB (50.0 μg), and LY54-XBB+P67-XBB (50.0+25.0 μg). On day 14 after the third immunization, mice were intranasally challenged with 3×10^3 $TCID_{50}$ of the SARS-CoV-2 BA.5 variant. The BA.5 variant was chosen for challenge because the vaccine elicited the highest neutralizing antibody titers against it in the cynomolgus monkey model. Lung tissues were collected on day 5 post-infection for viral load detection and pathological assessment (Figure 7A). Notably, the LY54-XBB&P67-XBB group showed significantly lower viral loads than the vehicle and the LY54-XBB groups (Figure 7B). Histopathological examination showed that the LY54-XBB group exhibited significant inflammatory cell infiltration around the pulmonary vasculature, involving a small number of pulmonary vessels, whereas the vehicle group showed increased perivascular spaces with three to four or more layers of inflammatory cells in the vascular sheaths and minimal granulocyte infiltration, affecting most pulmonary vessels and indicating parenchymal lesions in lung tissue. In contrast, the LY54-XBB&P67-XBB group exhibited minimal or almost no lung tissue abnormalities (Figure 7C-D). These results demonstrate the combined advantage of LY54-XBB and P67-XBB, as well as the protective effect of our vaccine in a human MHC system.

Validation of peptide T-cell immunogenicity in hPBMCs from CCP donors

To evaluate peptide immunogenicity in a human system, we used hPBMCs from CCP donors. IFN-γ responses were assessed by ELISpot after 24 h stimulation with peptides. Both peptides significantly increased the number of IFN-γ-secreting cells compared with the unstimulated control. The mixed peptide group did not induce a higher response than either single peptide, possibly due to the limited capacity of *ex vivo* antigen-presenting cells (APCs) (Figure 8A). Furthermore, intracellular cytokine staining was performed after 6 h incubation with peptides. Mixed peptides enhanced the production of TNF-α, IFN-γ, IL-4, and IL-6 in $CD4^+$ T cells (Figure 8B), as well as TNF-α, IFN-γ, IL-2, IL-4, and IL-6 in $CD8^+$ T cells (Figure 8C), and $CD8^+$ T-cell responses appeared to be slightly stronger.

In summary, both LY54-XBB and P67-XBB contain T-cell epitopes capable of potently inducing T-cell immune responses in hPBMCs, demonstrating their clinical potential

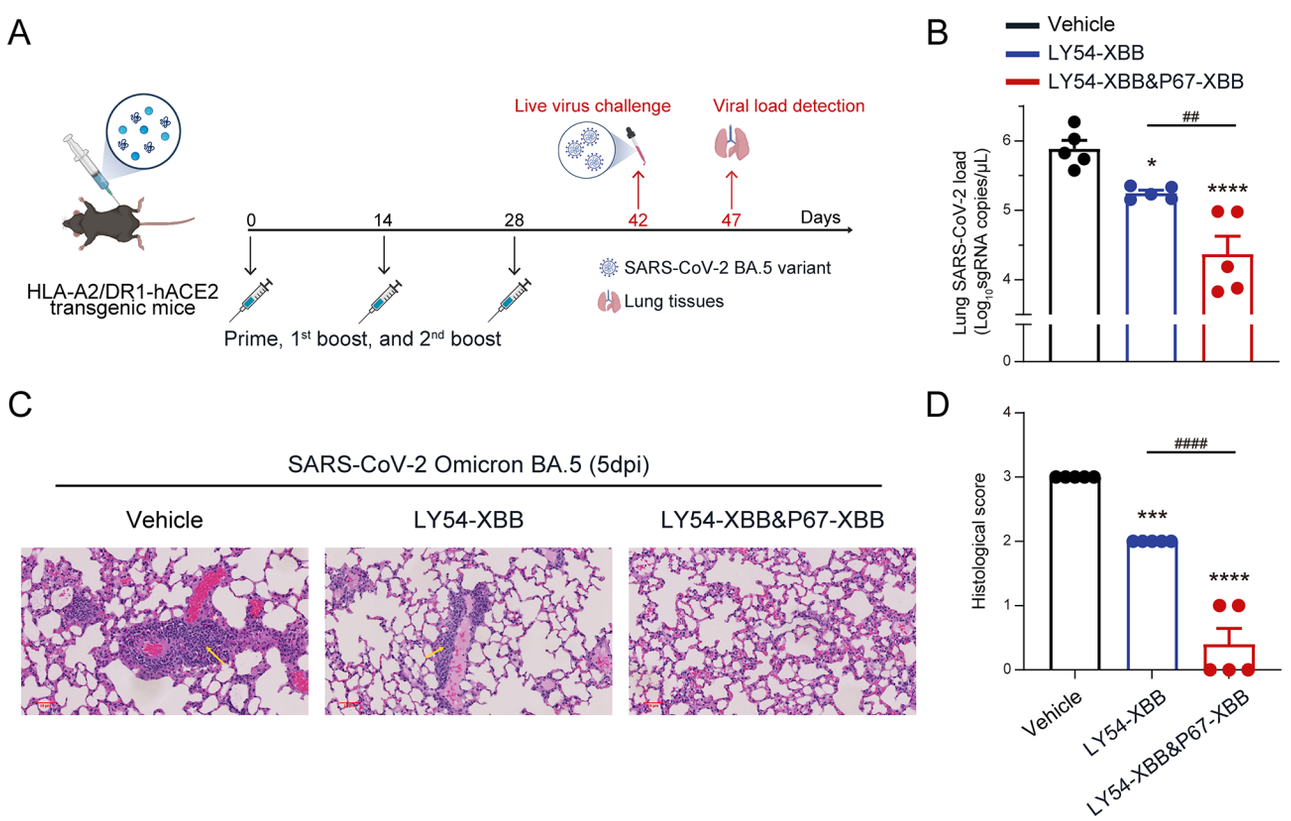

Figure 7 ***In vivo*** **protective efficacy against BA.5 induced by peptide vaccines**

A: Schematic diagram of the immunization and challenge experiments for peptide vaccines (*n*=5). B: Viral copy numbers in the lungs on day 5 post-infection (*n*=5). C: Lung tissue pathology was evaluated by H&E staining; scale bar, 200 μm (*n*=5). D: Pathological scores were calculated for each group of mice on day 5 post-infection (*n*=5). Data represent mean±SEM. For multiple group comparisons, one-way ANOVA followed by Tukey's or Dunnett's post-hoc test was applied as appropriate. *: $P<0.05$; ***: $P<0.001$; ****: $P<0.0001$; $^{\#\#}$: $P<0.01$; $^{\#\#\#\#}$: $P<0.0001$.

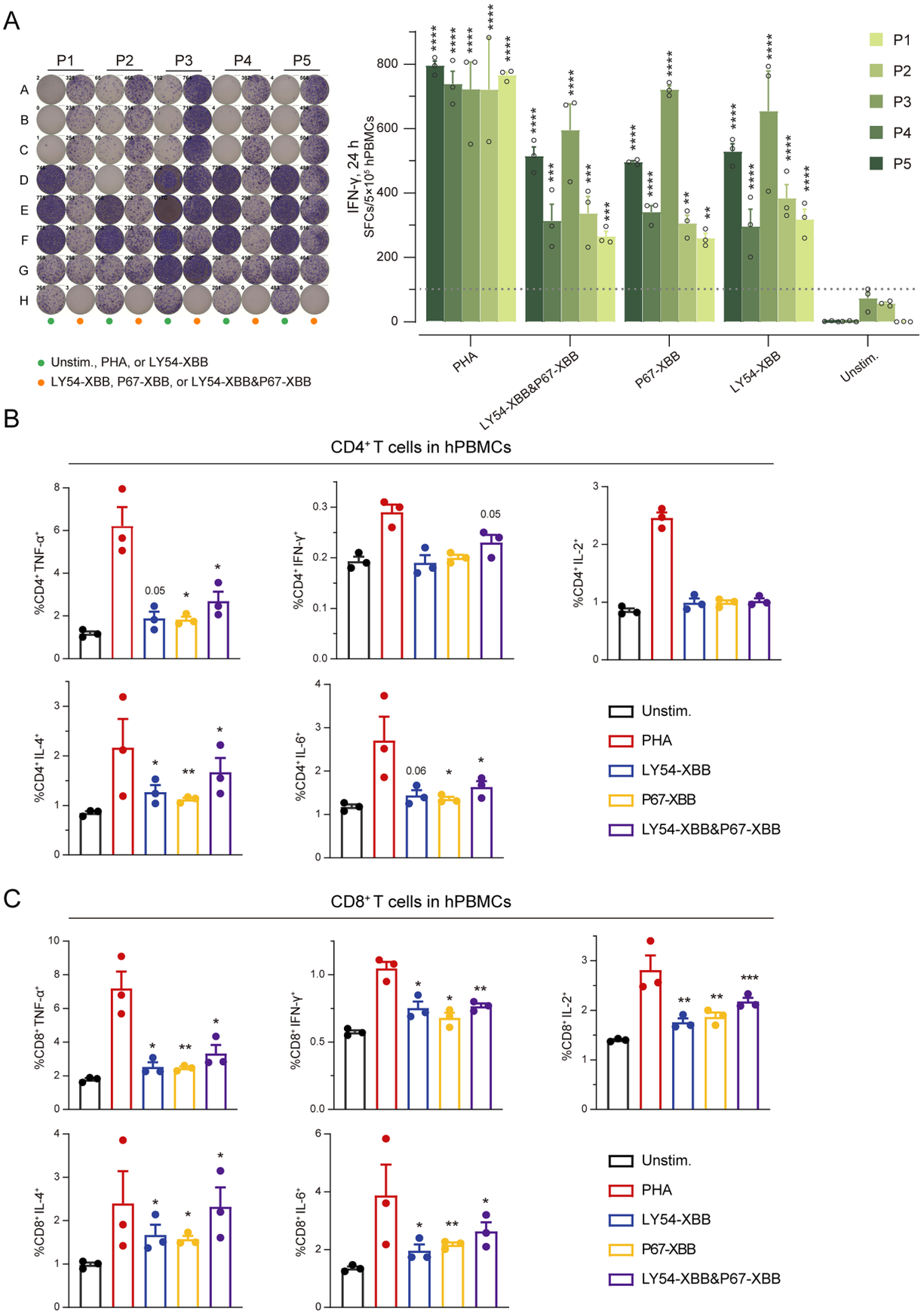

Figure 8 T-cell immune responses to peptides in hPBMCs

A: After hPBMCs from five CCP donors were co-cultured with peptides for 24 h, IFN-γ responses were detected by ELISpot (*n*=3). B: Peptide-specific T-cell responses were detected by flow cytometry, including TNF-α$^+$, IFN-γ$^+$, IL-2$^+$, IL-4$^+$, and IL-6$^+$ CD4$^+$ or CD8$^+$ T cells in hPBMCs (*n*=3). Data represent mean±SEM. For multiple group comparisons, one-way ANOVA followed by Tukey's or Dunnett's post-hoc test was applied as appropriate. *: P<0.05; **: P<0.01; ***: P<0.001; ****: P<0.0001.

for inducing cellular immunity.

Toxicity study of peptide vaccines in cynomolgus monkeys

At the study endpoint (day 63), comprehensive hematological and plasma biochemical analyses were performed in cynomolgus monkeys. Hematological parameters, encompassing complete blood counts (WBC, RBC, HGB, HCT, and PLT), erythrocyte indices (MCV, MCH, MCHC, and RDW), platelet profiles (MPV, PDW, P-LCR, and IPF), and leukocyte differentials (NEUT, LYMPH, MONO, EO, and BASO), remained within established physiological reference ranges for all groups (Supplementary Table S3) (Koga et al., 2005; Koo et al., 2019). Reticulocyte indices (RET, IRF, and RET-He) and absence of nucleated erythrocytes (NRBC) further supported undisturbed erythropoiesis and bone marrow homeostasis. Biochemical profiling (Supplementary Table S4) revealed no clinically relevant deviations in hepatic (ALT, AST, ALP, GGT, and TBIL), renal (CREA and UREA), metabolic (GLU, TC, and TG), or electrolyte markers (Na, K, Ca, P, and Cl) (Koga et al., 2005; Koo et al., 2019).

Collectively, these findings demonstrate that the vaccine candidates did not induce hematotoxicity (e.g., anemia or thrombocyte dysregulation) or systemic organ dysfunction (hepatic, renal, or metabolic), supporting their favorable safety profile in NHPs.

DISCUSSION

In this study, we applied an AI-aided epitope prediction strategy to develop a peptide vaccine containing two immunogenic regions within the RBDs of the SARS-CoV-2 Omicron subvariants. By integrating computational and experimental immunogenicity assays, we showed that our peptide vaccines elicited cross-reactive humoral and cellular immune responses, conferred protective efficacy against SARS-CoV-2 challenge, and induced antigen-specific cellular immune responses in hPBMCs *ex vivo*. These findings support the potential of this vaccine strategy as a rapidly adaptable booster platform against continuously evolving SARS-CoV-2 variants and other pathogens.

The rapid antigenic evolution of SARS-CoV-2, exemplified by the emergence of the immune-evasive XBB.1.5 variant, has diminished neutralization by many prior vaccines and therapeutics, emphasizing the need for adaptive, variant-focused vaccine strategies (Chemaitelly et al., 2025; Patel et al., 2023; Suzuki et al., 2022; Yue et al., 2023). Our vaccine strategy has the potential to address this challenge.

P67-XBB induced peptide-specific antibodies but did not induce SARS-CoV-2-specific antibodies, indicating that it contains epitopes recognizable by B cells. However, the absence of appropriate conformational epitopes may lead to the production of non-neutralizing or insufficiently protective antibodies, thereby limiting detectable immune responses to SARS-CoV-2 (Li et al., 2014, 2020). Therefore, further investigation of P67-XBB function remains necessary. Interestingly, P67-XBB is located in a reported class 3 neutralizing epitope of the RBD (non-ACE2-blocking, located on the side of the RBD and near residue N343) (Wibmer et al., 2021), including the Y351–R357 region (Li et al., 2021), suggesting that antibodies induced by P67-XBB may spatially influence the RBD conformation, thereby enhancing the neutralizing activity of antibodies induced by LY54-XBB, which acts as a conformational B-cell epitope. In addition, the P67-XBB may exhibit a carrier effect (Parker, 2013), providing auxiliary support to LY54-XBB by enhancing humoral and cellular immune responses.

Studies have shown that mutations may enable viruses to evade recognition by $CD8^+$ T cells, thereby weakening the cellular immune responses (Agerer et al., 2021). Therefore, cellular immune epitopes should not be overlooked in booster immunizations against emerging Omicron subvariants. In this study, we found that both peptides induced antigen-specific $CD4^+$ and $CD8^+$ T-cell immune responses. Combined with TCR-pMHC binding analysis, these findings indicated that P67-XBB contains more potential MHC epitopes. Booster immunization with P67-XBB may therefore supplement the strength and breadth of LY54-XBB-induced immune responses. By combining the advantages of the two peptides in humoral and cellular immunity, our findings support a low-dose, high-efficiency epitope synergy strategy (Sadarangani et al., 2021).

In *in vivo* NHP models, peptide vaccines induced a Th1-biased cellular immune response, which is required for antiviral immunity (Aleebrahim-Dehkordi et al., 2022) and is indicative of favorable safety characteristics (Ewer et al., 2021). No abnormal hematologic or biochemical parameters were observed in any peptide vaccine group, consistent with reports that peptide vaccines cause minimal toxicity and have a strong safety profile (Limeilati et al., 2024).

Several issues remain to be addressed in this study. First, recent analyses indicated that newly emerging BA.2.86 and JN.1 variants greatly reduce the antibody potency induced by the XBB.1.5 monovalent vaccine, especially against JN.1 (Li et al., 2024). In our study, a similar decrease in blocking ability against BA.2.86 and JN.1 was observed, demonstrating that our peptide vaccine was partially affected by viral immune escape. Therefore, we still need to assess neutralization against additional Omicron subvariants, including BA.2.86 and JN.1, despite detecting cross-reactive T-cell immune responses. The rapid design and production advantages of peptide vaccines could also be used to replace existing peptides with newly mutated peptide candidates for booster immunization. Second, the weakened humoral immune response against Omicron subvariants emerging after XBB.1.5 reflects antigenic drift, in which Omicron subvariants have accumulated numerous RBD point mutations that allow them to evade many antibodies (Yewdell, 2021). Encouragingly, other studies have shown that conserved epitopes can help overcome this drift (Chang et al., 2024). Therefore, future iterative antigenic epitope design using AI-aided vaccine design tools may enhance vaccine efficacy by targeting more conserved viral regions in addition to selecting immunogenic epitopes. To further validate the feasibility of our epitope design strategy, subsequent studies should assess the protective efficacy of the peptide vaccine against multiple Omicron subvariants through *in vivo* challenge experiments, *in vitro* live-virus neutralization assays, and related approaches, while also investigating the underlying immunological mechanisms of the peptides.

In summary, we employed an AI-aided epitope design strategy to develop a peptide vaccine containing T-cell and B-cell epitopes based on the RBD of XBB.1.5 and validated the strong immunogenicity of the peptides via *in silico*, *in vivo*, and *ex vivo* models. This epitope design strategy may be extended to peptide vaccine development against other pathogens.

SUPPLEMENTARY DATA

Supplementary data to this article can be found online.

COMPETING INTERESTS

The authors declare that they have no competing interests.

AUTHORS' CONTRIBUTIONS

K.Z.: Conceptualization, methodology, validation, formal analysis, investigation, data curation, writing-original draft, visualization. G.W.: Methodology, visualization. T.L.: Conceptualization, methodology, validation, formal analysis, investigation, data curation, writing-original draft, visualization. M.L.: Methodology, validation, formal analysis, data curation, writing-original draft. L.D.: Validation. Y.Z.: Validation. J.X.: Validation. H.L.: Validation. J.S.: Conceptualization, resources, supervision, funding acquisition. X.Z.: Resources. J.C.: Conceptualization, resources, supervision, project administration. G.Z.: Conceptualization, resources, supervision. X.G.: Conceptualization, resources, supervision. Y.L.: Conceptualization, resources, supervision, funding acquisition, validation, writing-original draft, project administration, writing-review, and editing. The manuscript was written through contributions of all authors. L.G.: Conceptualization, resources, supervision, funding acquisition, project administration. All authors read and approved the final version of the manuscript.

ACKNOWLEDGMENTS

All the schematics were created with BioRender.com.

REFERENCES

Abramson J, Adler J, Dunger J, et al. 2024. Accurate structure prediction of biomolecular interactions with AlphaFold 3. *Nature*, **630**(8016): 493–500.

Agerer B, Koblischke M, Gudipati V, et al. 2021. SARS-CoV-2 mutations in MHC-I-restricted epitopes evade $CD8^+$ T cell responses. *Science Immunology*, **6**(57): eabg6461.

Aguilar-Bretones M, Fouchier RAM, Koopmans MPG, et al. 2023. Impact of antigenic evolution and original antigenic sin on SARS-CoV-2 immunity. *The Journal of Clinical Investigation*, **133**(1): e162192.

Aleebrahim-Dehkordi E, Molavi B, Mokhtari M, et al. 2022. T helper type (Th1/Th2) responses to SARS-CoV-2 and influenza A (H1N1) virus: from cytokines produced to immune responses. *Transplant Immunology*, **70**(3): 101495.

Barchuk A, Cherkashin M, Bulina A, et al. 2022. Vaccine effectiveness against referral to hospital and severe lung injury associated with COVID-19: a case-control study in St. Petersburg, Russia. *medRxiv*, doi: https://doi.org/10.1186/s12916-022-02509-8.

Brochu H, Wang RH, Tollison T, et al. 2022. Alternative splicing and genetic variation of mhc-e: implications for rhesus cytomegalovirus-based vaccines. *Communications Biology*, **5**(1): 1387.

Chang TY, Li CJ, Chao TL, et al. 2024. Design of the conserved epitope peptide of SARS-CoV-2 spike protein as the broad-spectrum COVID-19 vaccine. *Applied Microbiology and Biotechnology*, **108**(1): 486.

Chemaitelly H, Ayoub HH, Coyle P, et al. 2025. Differential protection against SARS-CoV-2 reinfection pre- and post-Omicron. *Nature*, **639**(8056): 1024–1031.

Chen XT, Yang J, Wang LF, et al. 2020. Personalized neoantigen vaccination with synthetic long peptides: recent advances and future perspectives. *Theranostics*, **10**(13): 6011–6023.

Clifford JN, Høie MH, Deleuran S, et al. 2022. BepiPred-3.0: improved B-cell epitope prediction using protein language models. *Protein Science*, **31**(12): e4497.

Ewer KJ, Barrett JR, Belij-Rammerstorfer S, et al. 2021. T cell and antibody responses induced by a single dose of ChAdOx1 nCoV-19 (AZD1222) vaccine in a phase 1/2 clinical trial. *Nature Medicine*, **27**(2): 270–278.

Feng ZY, Chen JY, Hai YL, et al. 2024. Sliding-attention transformer neural architecture for predicting T cell receptor–antigen–human leucocyte antigen binding. *Nature Machine Intelligence*, **6**(10): 1216–1230.

Fornefett J, Krause J, Klose K, et al. 2018. Comparative analysis of clinics, pathologies and immune responses in BALB/c and C57BL/6 mice infected with *Streptobacillus moniliformis*. *Microbes and Infection*, **20**(2): 101–110.

He XC, Ding LF, Cao KL, et al. 2021. A human cell-based SARS-CoV-2 vaccine elicits potent neutralizing antibody responses and protects mice from SARS-CoV-2 challenge. *Emerging Microbes & Infections*, **10**(1): 1555–1573.

Heijmans CMC, De Groot NG, Bontrop RE. 2020. Comparative genetics of the major histocompatibility complex in humans and nonhuman primates. *International Journal of Immunogenetics*, **47**(3): 243–260.

Heitmann JS, Bilich T, Tandler C, et al. 2022. A COVID-19 peptide vaccine for the induction of SARS-CoV-2 T cell immunity. *Nature*, **601**(7894): 617–622.

Koga T, Kanefuji K, Nakama K. 2005. Individual reference intervals of hematological and serum biochemical parameters in cynomolgus monkeys. *International Journal of Toxicology*, **24**(5): 377–385.

Koo BS, Lee DH, Kang P, et al. 2019. Reference values of hematological and biochemical parameters in young-adult cynomolgus monkey (*Macaca fascicularis*) and rhesus monkey (*Macaca mulatta*) anesthetized with ketamine hydrochloride. *Laboratory Animal Research*, **35**: 7.

Li P, Faraone JN, Hsu CC, et al. 2024. Neutralization escape, infectivity, and membrane fusion of JN. 1-derived SARS-CoV-2 SLip, FLiRT, and KP. 2 variants. *Cell Reports*, **43**(8): 114520.

Li TT, Xue WH, Zheng QB, et al. 2021. Cross-neutralizing antibodies bind a SARS-CoV-2 cryptic site and resist circulating variants. *Nature Communications*, **12**(1): 5652.

Li WD, Joshi MD, Singhania S, et al. 2014. Peptide vaccine: progress and challenges. *Vaccines*, **2**(3): 515–536.

Li Y, Lai DY, Zhang HN, et al. 2020. Linear epitopes of SARS-CoV-2 spike protein elicit neutralizing antibodies in COVID-19 patients. *Cellular & Molecular Immunology*, **17**(10): 1095–1097.

Limeilati NA, Nidom RV, Sari TT, et al. 2024. Study of the immunogenicity, efficacy and safety of recombinant RBD SARS-CoV-2 vaccine with CpG adjuvant in rodent, non-rodent and Maccaca fascicularis using Indonesian strain virus. *BioRxiv*, doi: https://doi.org/10.1101/2024.12.18.629000.

Long YR, Sun JH, Song TZ, et al. 2022. CoVac501, a self-adjuvanting peptide vaccine conjugated with TLR7 agonists, against SARS-CoV-2 induces protective immunity. *Cell Discovery*, **8**(1): 9.

Malonis RJ, Lai JR, Vergnolle O. 2020. Peptide-based vaccines: current progress and future challenges. *Chemical Reviews*, **120**(6): 3210–3229.

Matveeva O, Ershov A. 2022. Retrospective cohort study of the effectiveness of the sputnik V and EpiVacCorona vaccines against the SARS-CoV-2 delta variant in moscow (June–July 2021). *Vaccines*, **10**(7): 984.

Nelde A, Rammensee HG, Walz JS. 2021. The peptide vaccine of the future. *Molecular & Cellular Proteomics*, **20**: 100022.

Nilsson JB, Kaabinejadian S, Yari H, et al. 2023. Accurate prediction of HLA class II antigen presentation across all loci using tailored data acquisition and refined machine learning. *Science Advances*, **9**(47): eadj6367.

Parker DC. 2013. The carrier effect and T cell/B cell cooperation in the antibody response. *The Journal of Immunology*, **191**(5): 2025–2027.

Patel P, Twentyman E, Koumans E, et al. 2023. Information for persons who are immunocompromised regarding prevention and treatment of SARS-CoV-2 infection in the context of currently circulating omicron sublineages - United States, January 2023. *Morbidity and Mortality Weekly Report*, **72**(5): 128–131.

Piccoli L, Park YJ, Tortorici MA, et al. 2020. Mapping neutralizing and immunodominant sites on the SARS-CoV-2 spike receptor-binding domain by structure-guided high-resolution serology. *Cell*, **183**(4): 1024–1042. e21.

Pompano RR, Chen JJ, Verbus EA, et al. 2014. Titrating T-cell epitopes within self-assembled vaccines optimizes CD4+ helper T cell and antibody outputs. *Advanced Healthcare Materials*, **3**(11): 1898–1908.

Reynisson B, Alvarez B, Paul S, et al. 2020. NetMHCpan-4.1 and

NetMHCIIpan-4.0: improved predictions of MHC antigen presentation by concurrent motif deconvolution and integration of MS MHC eluted ligand data. *Nucleic Acids Research*, **48**(W1): W449–W454.

Ryzhikov AB, Ryzhikov EA, Bogryantseva MP, et al. 2023. Assessment of safety and prophylactic efficacy of the EpiVacCorona peptide vaccine for COVID-19 prevention (Phase III). *Vaccines*, **11**(5): 998.

Sadarangani M, Marchant A, Kollmann TR. 2021. Immunological mechanisms of vaccine-induced protection against COVID-19 in humans. *Nature Reviews Immunology*, **21**(8): 475–484.

Schultheiß C, Paschold L, Simnica D, et al. 2020. Next-generation sequencing of T and B cell receptor repertoires from COVID-19 patients showed signatures associated with severity of disease. *Immunity*, **53**(2): 442–455. e4.

Shalash AO, Hussein WM, Skwarczynski M, et al. 2021. Key considerations for the development of safe and effective SARS-CoV-2 subunit vaccine: a peptide-based vaccine alternative. *Advanced Science*, **8**(16): 2100985.

Shi R, Shan C, Duan XM, et al. 2020. A human neutralizing antibody targets the receptor-binding site of SARS-CoV-2. *Nature*, **584**(7819): 120–124.

Smith CC, Olsen KS, Gentry KM, et al. 2021. Landscape and selection of vaccine epitopes in SARS-CoV-2. *Genome Medicine*, **13**(1): 101.

Su QD, Zou YN, Yi Y, et al. 2021. Recombinant SARS-CoV-2 RBD with a built in T helper epitope induces strong neutralization antibody response. *Vaccine*, **39**(8): 1241–1247.

Sun SH, Chen Q, Gu HJ, et al. 2020. A mouse model of SARS-CoV-2 infection and pathogenesis. *Cell Host & Microbe*, **28**(1): 124–133. e4.

Suzuki R, Yamasoba D, Kimura I, et al. 2022. Attenuated fusogenicity and pathogenicity of SARS-CoV-2 Omicron variant. *Nature*, **603**(7902): 700–705.

Tandler C, Heitmann JS, Michel TM, et al. 2024. Long-term efficacy of the peptide-based COVID-19 T cell activator CoVac-1 in healthy adults. *International Journal of Infectious Diseases*, **139**: 69–77.

Vangone A, Spinelli R, Scarano V, et al. 2011. COCOMAPS: a web application to analyze and visualize contacts at the interface of biomolecular complexes. *Bioinformatics*, **27**(20): 2915–2916.

Villanueva-Flores F, Sanchez-Villamil JI, Garcia-Atutxa I. 2025. AI-driven epitope prediction: a systematic review, comparative analysis, and practical guide for vaccine development. *npj Vaccines*, **10**(1): 207.

Wang CY, Hwang KP, Kuo HK, et al. 2022. A multitope SARS-CoV-2 vaccine provides long-lasting B cell and T cell immunity against Delta and Omicron variants. *The Journal of Clinical Investigation*, **132**(10): e157707.

Wang XL, Yuen TTT, Dou Y, et al. 2023. Vaccine-induced protection against SARS-CoV-2 requires IFN-γ-driven cellular immune response. *Nature Communications*, **14**(1): 3440.

Wibmer CK, Ayres F, Hermanus T, et al. 2021. SARS-CoV-2 501Y. V2 escapes neutralization by South African COVID-19 donor plasma. *Nature Medicine*, **27**(4): 622–625.

Xiao WJ, Jiang WJ, Chen Z, et al. 2025. Advance in peptide-based drug development: delivery platforms, therapeutics and vaccines. *Signal Transduction and Targeted Therapy*, **10**(1): 74.

Xue Y, Yang D, Vogel P, et al. 2022. Cardiopulmonary injury in the Syrian hamster model of COVID-19. *Viruses*, **14**(7): 1403.

Yewdell JW. 2021. Antigenic drift: understanding COVID-19. *Immunity*, **54**(12): 2681–2687.

Yin R, Ribeiro-Filho HV, Lin V, et al. 2023. TCRmodel2: high-resolution modeling of T cell receptor recognition using deep learning. *Nucleic Acids Research*, **51**(W1): W569–W576.

Yue C, Song WL, Wang L, et al. 2023. ACE2 binding and antibody evasion in enhanced transmissibility of XBB. 1.5. *The Lancet Infectious Diseases*, **23**(3): 278–280.